13th International Symposium on Particle Image Velocimetry – ISPIV 2019
Munich, Germany, July 22-24, 2019

Inverse technique for Lagrangian, non-Stokesian tracer particle correction

Joshua N. Galler[1]* and David E. Rival[1]

[1] Queen's University, Department of Mechanical and Materials Engineering, Kingston, Canada

* j.galler@queensu.ca

Abstract

A kinetic-energy-based approach to modeling unsteady forces on an accelerated sphere is implemented for the purpose of fluid velocity extraction with non-Stokesian tracer particles. An expression for the force due to the energized-mass concept of Galler et al. (under review) is developed, with contributions due to rate of shear-layer growth and quasi-steady drag. The model exhibited strong agreement with 2D particle image velocimetry and direct force measurements performed for two cases of an accelerated sphere. The dynamic model was applied to the case of a non-ideal particle responding to a velocity perturbation, with a relative velocity between the body and fluid. Compared to the velocity response predicted by conventional force models, the energized mass model resulted in additional force, and therefore greater acceleration, during the change in fluid velocity. The relaxation to steady state was then slowed due to the relative acceleration between the body and steady flow.

1 Introduction

Large-scale particle image velocimetry (LS-PIV) and large-scale particle tracking velocimetry (LS-PTV) are required for the study of flows such as the atmospheric boundary layer (ABL), where *in situ* measurement domains are on the order of 10×10 m^2 (Nemes et al., 2017). Rosi et al. (2014) and Toloui et al. (2014) characterized mean properties of the atmospheric boundary layer (ABL) using an LS-PTV system with soap bubble tracers and LS-PIV using natural snowfall as tracers, respectively. In addition, Terra et al. (2017) exhibited success measuring drag with hydrogen-filled soap bubbles in a wind tunnel, however their measurement domain was much smaller than those characteristic of the ABL. Large particles have been shown to provide sufficient response for estimation of mean flow properties over very large measurement domains however, velocity perturbations remain a challenge due to the particles' non-Stokesian time-response. To mitigate the error due to time-lag associated with an inertial response, dynamic modeling of the tracer particle's motion allows for a flow velocity correction, where the true flow velocity can be "backed-out" from measured particle trajectories.

Classical force modeling techniques decompose the force response of a body into acceleratory, steady, and history effects, as summarized by Odar and Hamilton (1964) in their low Reynolds number investigation of forces on a sphere. The acceleratory and steady components of the force have been described by Theodorsen (1935) and von Kármán and Sears (1938) in the terms of non-circulatory and circulatory forces, where fluid inertia and added-mass comprise the non-circulatory component of the force, while bound and wake vortices make up the quasi-steady component. Such a breakdown of the forces has inspired contemporary models for the estimation of forces in viscous flows (Baik et al., 2012; Graham et al., 2017), however, the applicability of potential-flow added-mass to force modeling in separated flow remains in question. The ability of large-scale particle tracking techniques to extract information from unsteady flows is hindered by the limitations of available low-order models.

The current study presents a kinetic-energy based approach to modeling unsteady forces on a heavy spherical tracer. Experimental results are used to validate the model for a basic case, before extension to the more complex scenario of an inertial particle subject to a changing freestream velocity. The modeled velocity response of a non-Stokesian test article is presented and compared with predictions from classical dynamic

models. The ultimate goal of the presented modeling approach is the extraction of fluid velocity from the inertial response of a non-Stokesian tracer particle.

2 Tracer particle response modeling

In this section, particle response to velocity perturbations will be discussed, and the modeling technique developed for particle response correction.

2.1 Classical models of particle time-response

The net force on a tracer particle is defined as the particle mass times acceleration. Assuming buoyancy and gravitational forces to be negligible, the net force is then solely due to the drag force on the body. Classically, Stoke's flow is assumed for tracer particles, which show near-perfect flow-fidelity. The drag force for a sphere in Stokes' flow is written as:

$$D = 6\pi\mu R(u-U). \tag{1}$$

Stokes' drag is generally appropriate for traditional tracer particles, which typically experience low Reynolds number regimes and are of Stokes number less than one. For large tracer particles, such as bubbles or natural snowfall, the Stokes drag assumption breaks down due to their large size and significant density relative to air. In such regimes, the classical force breakdown into quasi-steady and added mass components can be used (Brennen (1982)). Quasi-steady drag force is defined in the familiar form as:

$$D = \frac{1}{2}C_D\rho(u-U)\pi R^2. \tag{2}$$

For unsteady problems with significant acceleration, an added mass force is added to the quasi-steady drag to model the acceleration of the fluid due to the body. The additional force contribution is written as:

$$D = \frac{1}{2}C_D\rho(u-U)\pi R^2 + \frac{4}{3}\rho\pi R^3 K\frac{d(u-U)}{dt}, \tag{3}$$

where K is the added mass coefficient for a sphere. The linear addition of quasi-steady drag and potential-flow added-mass forces has been shown to suffer from significant error when compared to experiment. The limits of added mass theory were evaluated by Fernando et al. (in press), who experimentally investigated the force on a circular flat plate for several acceleration moduli at high Reynolds number. A discrepancy between measured and analytically determined values was reported when comparing direct force measurements to forces modeled by Equation 3. When the model was compared to experimental results, up to 40% of the measured peak force was not accounted for by the force model. At the limit of impulsive motions, where potential theory should be most applicable, the discrepancy asymptoted to 20%. An alternative approach to unsteady force estimation is necessary for systems involving separated flow.

2.2 Energized-mass framework

A kinetic-energy-based force model (Galler et al., under review) has shown promise for an accelerated circular disk, a canonical test case characteristic of flow separation during a rapid acceleration. The same framework can be applied to a spherical particle experiencing a gust, shown schematically in Figure 1(a). A particle of radius R and mass M will experience a drag force D due to an impinging gust, $u(t)$. In turn, the particle will accelerate and move at some velocity, $U(t)$. The time trace of the gust is shown schematically in Figure 1(b), where the gust is comprised of two stages. First, a ramp of time length, τ_g, during which the flow velocity increases from zero to a final velocity, U_f. Figure 1(c) and (d) present a conceptual schematic for energized mass formation during the motion, showing how the energized mass evolves in time.

Galler et al. (under review) showed a region of energized fluid that developed around the plate, and the amount of "energized mass" was measured in time. The force was decomposed into two terms, as shown in Equation 4:

$$F(t) = \frac{\partial m_e}{\partial t}U + m_e\frac{\partial U}{\partial t}, \tag{4}$$

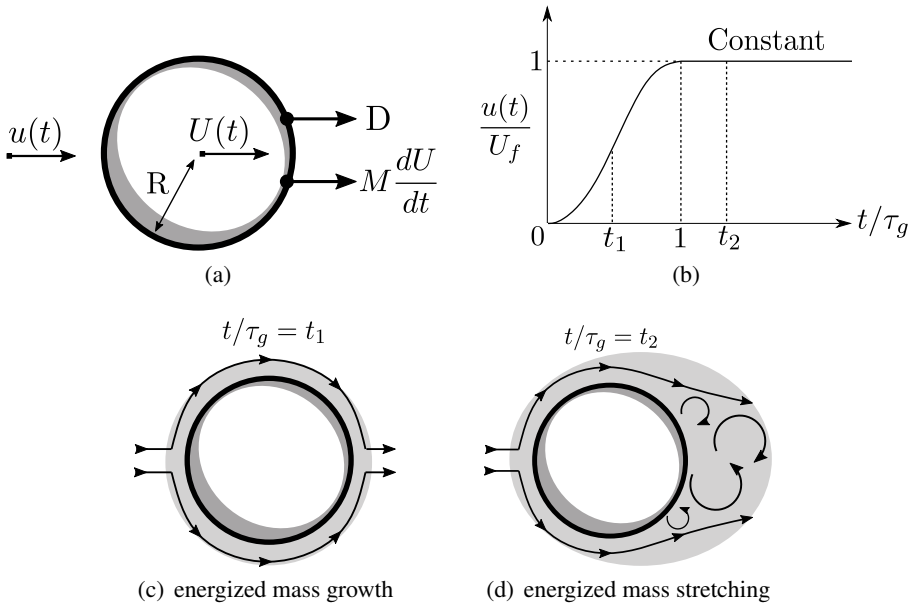

Figure 1: Schematics outlining the tracer particle-gust system: (a) The model evaluates the velocity response, $U(t)$, of the tracer particle, which experiences a drag force of D due to an impinging (uniform) gust front of velocity $u(t)$. (b) $u(t)$ represents the linear gust ramp followed by a steady velocity. (c) and (d) Schematic of energized mass growth for a sphere impulsively started from rest between arbitrary time steps. Time t_1 is during the early phase of acceleration, where the flow is still attached, and the energized mass is a small region close to the body. Time t_2 shows a later stage of the motion. Flow has separated, and the energized mass region has stretched downstream, while the region upstream of the body has changed little.

where m_e is the instantaneous energized mass, U is the body velocity and t is time. The energized mass method showed good agreement with direct force measurements, proving its viability as a force-estimation technique.

For the case of a large tracer particle responding to a gust, the energized mass approach can be used to solve for the flow velocity by modifying Equation 4 for the case of a "slip" or relative velocity between the body and surrounding fluid. The differential equation that describes the motion of the sphere is written in Equation 5, where M is the mass of the body, U is the body velocity and u is the flow velocity:

$$M\frac{\partial(U)}{\partial t} = \frac{\partial m_e}{\partial t}(u-U) + m_e\frac{\partial(u-U)}{\partial t}. \tag{5}$$

To satisfy Equation 5 and compute $u(t)$, the energized mass must be known or predicted. An analytical model for the energized mass growth is proposed:

$$m_e(t) = \int_0^{\tau}\frac{1}{2}C_d\rho A(u-U)dt + \int_0^{\tau}\rho\frac{4}{3}\pi((R+d(t))^3 - R^3)\frac{1}{(u-U)}\frac{\partial(u-U)}{\partial t}dt, \tag{6}$$

where A is the projected area of the sphere, C_d is the drag coefficient, and d is the shear layer thickness, as defined by Brown and Roshko (1974). Both terms are integrated over τ, the time period of interest. The first term accounts for the steady accumulation of kinetic energy in the fluid, proportional to the body velocity and drag coefficient. Logically, this term must be equal to the quasi-steady kinetic energy at the limit of steady motion, and has been written as such. The second term is the accumulation of energized mass in the developing shear layer, modeled by the shear layer mass flow rate. The shear layer volume is modeled as a spherical shell of fluid around the body with an experimentally-determined thickness. As the shear layer forms, proportional to the acceleration and velocity, kinetic energy is transferred to the fluid and the energized mass grows. Modeling the affect of body acceleration in this manner encapsulates the effect of viscosity. Compared to potential-flow added mass, which is a constant proportional to the displaced fluid mass, the energized mass is allowed to grow in time, incorporating the history of the fluid.

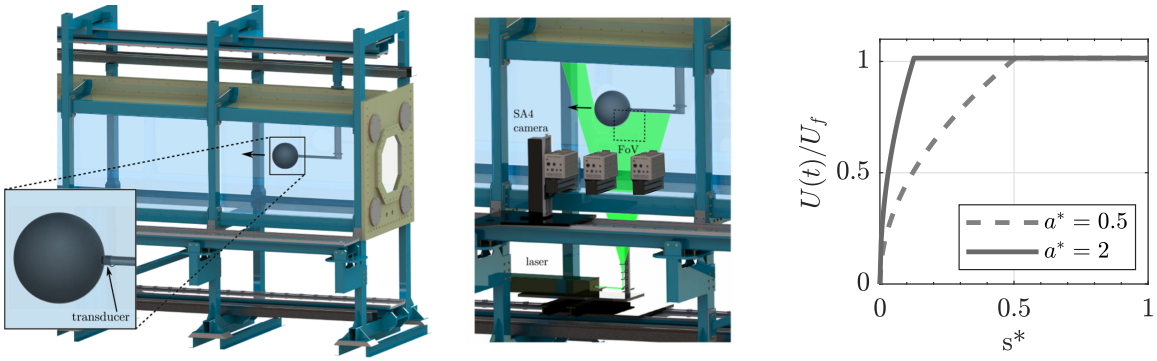

(a) facility schematic (b) PTV setup (c) test case velocity profiles

Figure 2: a) Towing tank facility showing the sphere mounted to the sting and submerged in the tank. The inset shows the location of the force transducer. b) Experimental setup showing the location of the cameras, laser sheet and field of view (FoV). c) Velocity profiles for the two cases studied. The acceleration occurs over $s = 0.5$D and $s = 0.125$D, after which the body was towed at a steady velocity.

3 Experimental methods

To apply the kinetic-energy-based approach to large tracer particles, the energized mass of a sphere was measured using 2D-PTV. Experiments were performed in the optical towing tank facility at Queen's University. The facility has a cross sectional area of 1 m^2, and total length of 15 m. The sphere, with diameter $D = 0.25$ m, was towed from rest to a final Reynolds number of 50,000 for acceleration moduli, $a^* = aD/U_f^2$ of 0.5 and 2, motions representative of large amplitude and rapid velocity perturbations (Fernando et al., 2017). Force was measured using a six-component, ATI Nano force transducer, with a static resolution of 0.125 N. Three Photron SA4 high-speed cameras, with resolutions of 1024 x 1024 px were used to capture the flow field. A 40 mJ per pulse Photonics Nd:YLF high-speed laser was used to produce an approximately 2 mm thick laser sheet in the xy-plane. The field of view for each individual camera measurement was $1.2D$ x $1.2D$ in size and located at the horizontal midspan of the sphere along the lower half of the sting, as shown in Fig.2. The fields of view were stitched together for a total field of view of $3.6D$ x $1.2D$ in size.

4 Results and discussion

4.1 Measurement and prediction of energized mass

Figure 3 shows the region of energized fluid around the sphere visible in the PTV snapshot for two instances in time for the $a^* = 2$ case. For brevity, a snapshot of the $a^* = 0.5$ case has been omitted as the topology is qualitatively similar. The evolution of the energized mass in time can be seen in Figure 4. There exists a clear trend in the growth of the energized mass that can be separated into two phases, marked by the kink in the curve that occurs at the end of acceleration. The first phase is dominated by the effects of acceleration while the second is composed of the wake development and relaxation to steady state. The slope of the second phase eventually converges to the steady rate of energy transfer between the body and the fluid.

Using Equation 6, the energized mass history of the sphere was predicted for both cases measured experimentally, shown in Figure 4. The trends of the energized mass growth are captured, however there are significant discrepancies that should be noted. After completing the acceleration, the experimental data shows a relaxation period over which the flow reaches steady state, which has been shown to be dictated by vortex roll-up and steady wake formation (Fernando et al. (2017)). The model does not capture the relaxation phase because it is purely a function of body kinematics. Modification of the terms or coefficients to account for the time associated with wake formation would benefit the model with respect to capturing the energized mass associated with the relaxation period. With the modeled energized mass, the forces can be predicted, as shown in Figure 5. Strong agreement is seen with directly measured forces, though the same discrepancies are present as with the energized mass prediction. The relaxation and wake formation phases

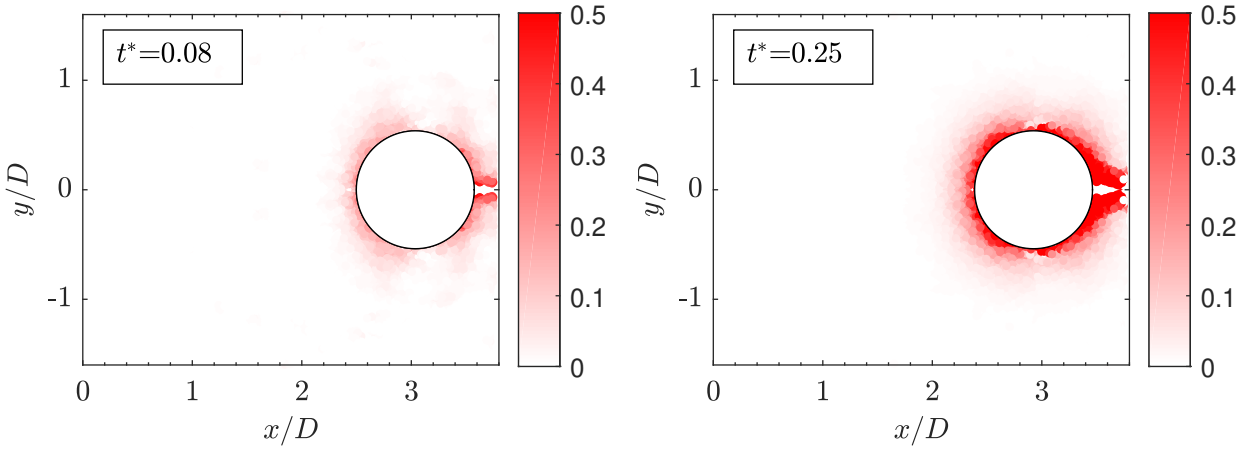

(a) energized mass field during acceleration

(b) energized mass field post acceleration

Figure 3: Particles coloured by instantaneous kinetic energy non-dimensionalized by body kinetic energy visualize the energized mass of fluid growing around the plate, shown for the $a^* = 2$ case.(a) The energized mass region forms around the sphere during the acceleration phase. (b) The sphere has completed its acceleration at $t^* = 0.25$ and the energized mass region has begun to stretch downstream. The upstream energized mass region covers a similar area as the previous snapshot, but has increased in magnitude.

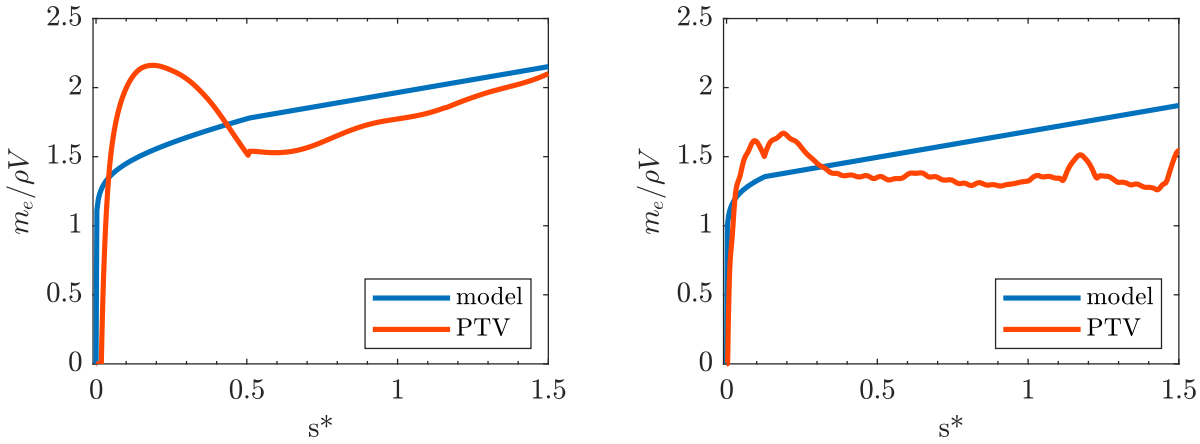

(a) Re $= 50,000$ $a^* = 0.5$

(b) Re $= 50,000$ $a^* = 2$

Figure 4: Modeled and measured energized mass plotted against non-dimensionalized displacement, $s*$. The energized mass has been non-dimensionalized by the displaced fluid volume of the body. (a) $a^* = 0.5$ and (b) $a^* = 2$ show similar energized mass magnitudes but differ in the slope during the acceleration and relaxation. The model captures the trends of measured energized mass growth but with clear discrepancies during the relaxation period.

are neglected, and will require model modification to more accurately capture. Notably, the model is able to predict a rise to the force peak, with some overshoot.

To the end of velocity extraction, the model has been applied to the time-response of a sphere subject to a non-dimensionalized gust of wavelength 1D, presented in Figure 6. A sphere with diameter of 5 cm and mass of 0.1 grams was simulated as an arbitrarily large and heavy test article, representative of the test article to be used in future experiments. Evidently, the tracer accelerates quickly during the gust before relaxing to a quasi-steady rise to the freestream. Compared to the conventional added-mass model, the energized mass approach predicts a faster acceleration and exhibits an additional effect on the response of the sphere during

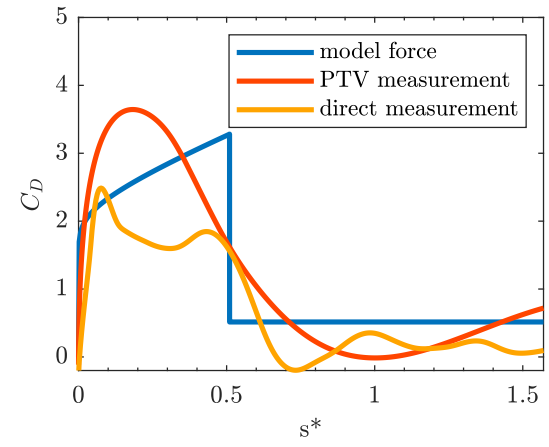

(a) Re $= 50,000$ $a^* = 0.5$

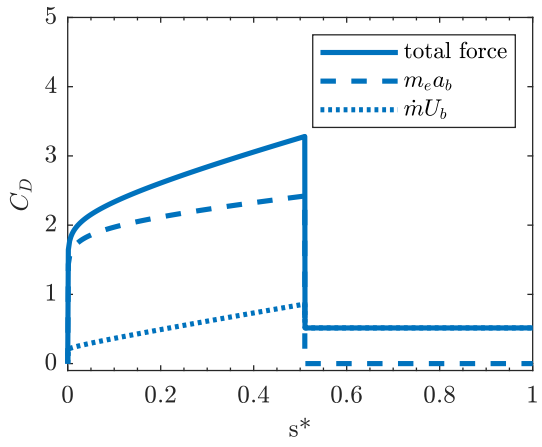

(b) Re $= 50,000$ $a^* = 0.5$

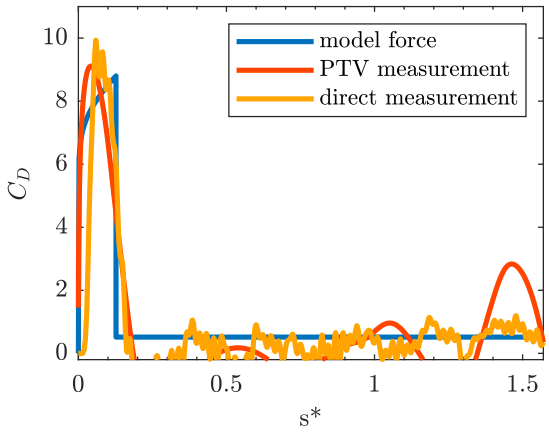

(c) Re $= 50,000$ $a^* = 2$

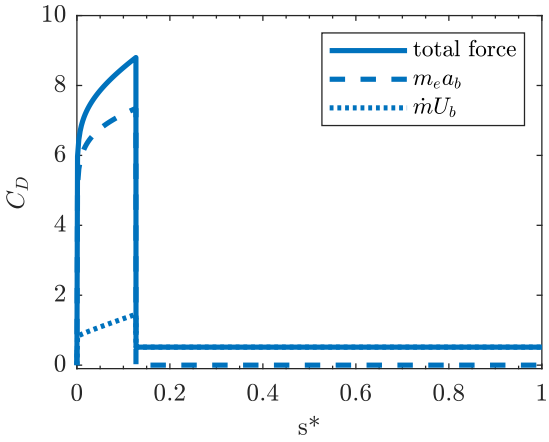

(d) Re $= 50,000$ $a^* = 2$

Figure 5: (a) and (c) Modeled force history plotted against non dimensionalized displacement, $s*$ and compared to forces obtained via force balance, and PTV data for $a^* = 0.5$ and $a^* = 2$ respectively. (b) and (d) The predicted force broken down into acceleration and rate of change of mass terms from Equation 4. Note the relative contributions from the rate of change of mass term and acceleratory terms, showing the contribution from the rate of change of energized mass. The main trends of the sphere force response are captured by the model, however the relaxation phase is clearly omitted.

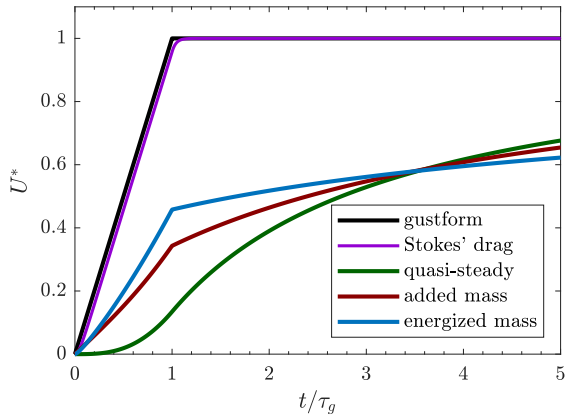

Figure 6: Tracer response to a gust using energized-mass-based model compared to the potential-flow added mass model of Equation 4. Note the enhanced response of the energized-mass model, predicting a faster rise in tracer velocity, due to the rapid increase in forces. As the tracer relaxes, a slower climb to freestream velocity follows.

the steady component of the gust, impeding its rate of acceleration to the freestream velocity. Additionally, Stokes' drag predicts an unrealistic response, as expected. Finally, considering only quasi-steady drag results in a response that lags behind the other models during the acceleration. Once the gust has reached steady-state, the quasi-steady model over-predicts the body's acceleration due to the lack of a relative acceleration term. Experimental validation is in progress.

5 Conclusions and outlook

An energized-mass approach to force estimation was applied to the response of a non-Stokesian tracer particle experiencing a rapid velocity perturbation for applications to fluid velocity extraction from measured tracer trajectories. A model for the growth of energized mass was proposed, comprised of quasi-steady and acceleratory mass accumulation. Two terms were used in the expression, one proportional to shear layer growth, and a second proportional to the instantaneous body velocity and drag coefficient. The predicted energized mass time-history and resultant forces agreed well with experimental results for a sphere accelerated from rest, with expected discrepancies during the relaxation phase of the flow. Energized mass growth can be sufficiently described by shear-layer formation during the acceleration phase, and quasi-steady energy transfer thereafter. The proposed model was used to predict the velocity response of a large tracer and compared against conventional force modeling techniques for a strong velocity perturbation. The energized-mass approach predicted a greater acceleration during the gust phase, before an impeded climb to the freestream velocity. Optical measurements of the trajectory of a sphere free to respond to a gust are currently underway to validate model predictions and evaluate the accuracy of the inverse technique.

Acknowledgements

JNG and DER wish to thank the Natural Sciences and Engineering Research Council of Canada for their financial support.

References

Baik YS, Bernal LP, Granlund K, and Ol MV (2012) Unsteady force generation and vortex dynamics of pitching and plunging aerofoils. *Journal of Fluid Mechanics* 709:37–68

Brennen CE (1982) A review of added mass and fluid inertial forces.. Technical report. Department of the Navy

Brown GL and Roshko A (1974) On density effects and large structure in turbulent mixing layers. *Journal of Fluid Mechanics* 64:775–816

Fernando JN, Marzanek M, Bond C, and Rival DE (2017) On the separation mechanics of accelerating spheres. *Physics of Fluids* 29

Fernando JN, Weymouth GD, and Rival DE (in press) On the limits of added-mass theory in separated flows and with varying initial conditions. *Journal of Fluids and Structures*

Galler JN, Weymouth GD, and Rival DE (under review) Energized mass: A realistic estimate of fluid forces in separated flows. *Journal of Fluid Mechanics*

Graham WR, Ford CP, and Babinsky H (2017) An impulse-based approach to estimating forces in unsteady flow. *Journal of Fluid Mechanics* 815:60–76

Nemes A, Dasari T, Hong J, Guala M, and Coletti F (2017) Snowflakes in the atmospheric surface layer: observation of particle-turbulence dynamics. *Journal of Fluid Mechanics* 814:592–613

Odar F and Hamilton WS (1964) Forces on a sphere accelerating in a viscous fluid. *Journal of Fluid Mechanics* 18:302–314

Rosi GA, Sherry M, Kinzel M, and Rival DE (2014) Characterizing the lower log region of the atmospheric surface layer via large-scale particle tracking velocimetry. *Experiments in Fluids* 55:1736

Terra W, Sciacchitano A, and Scarano F (2017) Aerodynamic drag of a transiting sphere by large-scale tomographic-piv. *Experiments in Fluids* 58

Theodorsen T (1935) General theory of aerodynamic instability and the mechanism of flutter. *NACA Report* pages 2–21

Toloui M, Riley S, Hong J, Howard K, Chamorro L, Guala M, and Tucker J (2014) Measurement of atmospheric boundary layer based on super-large-scale particle image velocimetry using natural snowfall. *Experiments in Fluids* 55:1737

von Kármán T and Sears WR (1938) Airfoil theory for non-uniform motion. *Journal of the Aeronautical Sciences* 5:379–390